

Research article

Construction of a thermally conductive network to improve the thermal and mechanical performance of silicone rubber foam

Hongjie Xie¹, Lijuan Zhao¹, Yanli Chen¹, Bing Han², Yu Hua², Dongliang Zhang², Zhaoqiang Li², Qibo Deng^{3,4}, Yunfeng Zhao^{1*} 

¹School of Materials Science and Engineering, Tianjin University of Technology, 300384 Tianjin, China

²Suzhou Techinno New Materials Technologies Co., Ltd., 215500 Changshu, Jiangsu, China

³Key Laboratory of Hebei Province on Scale-span Intelligent Equipment Technology, Tianjin Key Laboratory of Power Transmission and Safety Technology for New Energy Vehicles, and School of Mechanical Engineering, Hebei University of Technology, 300401 Tianjin, China

⁴Advanced Equipment Research Institute Co., Ltd. of HEBUT, 300401 Tianjin, China

Received 17 May 2023; accepted in revised form 20 August 2023

Abstract. Silicone foam (SF) is a porous silicone rubber with a lower density, higher elasticity, and good thermal stability. In this work, we selected aluminum spheres and carbon fiber (CF) as thermally conductive fillers to prepare hybrid SF. After optimization, we found that Al and CF hybrid SF (Al-CF-SF) has a higher thermal conductivity ($1.37 \text{ W}\cdot\text{m}^{-1}\cdot\text{K}^{-1}$) than the single-filler filled SF (CF-SF, $1.2 \text{ W}\cdot\text{m}^{-1}\cdot\text{K}^{-1}$ or Al-SF, $0.52 \text{ W}\cdot\text{m}^{-1}\cdot\text{K}^{-1}$) under the same filling amount of 60 wt%. The finite element simulation was used further to explore the thermal conductive mechanism of the hybrid SF. Meanwhile, the compressive and tensile modulus of the material (CF-SF) was increased to 10.8 and 3.3 MPa compared with pure SF, respectively, and the mechanical properties were improved. In addition, infrared thermography further demonstrated that Al-CF-SF has a faster heat transfer rate under relaxation and applied pressure.

Keywords: polymer composites, mechanical properties, thermal properties, silicone foam, hybrid filler

1. Introduction

Polymer foam is a kind of functional polymer with many pores inside [1]. Due to their unique cellular structure properties, lower weight and mechanical damping make the foams attractive in many applications [2, 3]. Specially, silicone rubber foam (SF) possesses the advantages of flexibility, electrical insulation and excellent chemical and thermal stability [4, 5] and many applications in energy absorption and insulation [6–8]. However, the presence of a large number of cellular structures causes the foam to turn into thermal insulation and destroy its mechanical strength which limits the use of foam in situations

where both mechanical damping and thermal conductivity requirements [9, 10], such as the battery and the sensors of vehicles.

Adding high thermal conductivity (K) fillers to the polymer matrix is an effective way to improve thermal conductivity [11, 12]. Li *et al.* [13] proposed a simple foaming method to immobilize the thermal conductive pathway using the gelation of cured polysaccharides under heating conditions, and a high K of $1.253 \text{ W}\cdot\text{m}^{-1}\cdot\text{K}^{-1}$ was recorded from a 3D- Al_2O_3 -PDMS composite with high alumina loading (69.6 wt%) prepared by vacuum-assisted impregnation. Zhang *et al.* [14] synthesized a carbon nanotube

*Corresponding author, e-mail: yfzhao@tjut.edu.cn

© BME-PT

and graphene oxide composite 3D network by a simple self-assembly process to prepare foam composites, and the results showed that the electrical, thermal, and mechanical properties of the composites could be effectively improved [15, 16]. The type and proportion of fillers affect the constructive effect of thermal conductive networks, and the synergistic effect of mixed fillers is closely related to the magnitude of thermal conductivity [17–19].

The purpose of this paper is to utilize the shock-absorbing properties of silicon foam to reduce the damage to electronic components in the collision process, and the heat can be quickly transferred out simultaneously. It has been reported that the combination of one-dimensional carbon fiber and particles with high K makes it easier to obtain a continuous structure with high thermal conductivity [20]. Therefore we designed a series of hybrid SF filled with high K fillers of Al powder ($230 \text{ W}\cdot\text{m}^{-1}\cdot\text{K}^{-1}$) [21, 22] and the carbon fiber (CF, $900 \text{ W}\cdot\text{m}^{-1}\cdot\text{K}^{-1}$) [23, 24] to investigate the relationship between fillers and thermal conductivity of SF composites. It was found that the thermal and mechanical properties of SF filled with different sizes of Al (5, 10 and $30 \mu\text{m}$) and CF were improved. In addition, we constructed a more efficient thermal conductive pathway using the filler synergy between Al powder and CF, and the optimized Al-CF-SF composite obtained the highest K ($1.37 \text{ W}\cdot\text{m}^{-1}\cdot\text{K}^{-1}$). Infrared thermography also showed that the increase in the filler amount and external pressure favored the heat transfer rate of SF composites.

2. Experimental section

2.1. Materials

Liquid silicone rubber (F663A and F663B) was supplied by Hongyejie Technology Co., Ltd. (Guangdong, China). Mix component A and component B

in a 1:1 ratio, with a foaming coefficient of three times. Short-cut carbon fibers (CF, >99%) with a diameter of $45 \mu\text{m}$ and a length of $7\text{--}10 \mu\text{m}$ were procured from Cangzhou Zhongli New Material Technology Co., Ltd. (Hebei, China). Aluminum powders with purity of 99.9% were supplied by Ansteel Group Aluminum Powder Co., Ltd. (Liaoning, China). In this article, three different particle sizes of Al powders of 5, 10, and $30 \mu\text{m}$ were used as fillers. All chemical reagents used in this paper were analytically pure and did not require further purification at the time of use.

2.2. Composite preparation

First, component A was prepared by mixing hydroxyl-containing silicone oil and Karstedt catalyst for two minutes. Similarly, component B consists of hydrogen-containing silicone oil and an inhibitor. Component A was mixed with component B in a weight ratio of 1:1, and the H-containing silicone oil and the OH-silicone oil reacted in the presence of the catalyst to produce hydrogen (H_2), and H_2 also acts as a foaming agent. And then, the mixture is put in the middle of two glass plates, and pressed down by four weights (1 kg) on the top plate. Finally, the glass plate was transferred to an oven for heat treatment at 30°C for 24 h for foaming. We named the silicone rubber foam prepared without any fillers SF. For the hybrid SF, the thermally conductive filler (CF/Al) is uniformly mixed with component A/B through mechanical stirring. The other steps are the same as the preparation of SF. According to the type and content of fillers, the naming of hybrid SF is detailed in Table 1.

2.3. Characterization

Scanning electron microscopy (SEM) images were obtained by using a field emission electron microscope (FEI-Quanta FEG 250, USA). Before shooting

Table 1. The formulation of the SF, Al-SF, CF-SF, and Al-CF-SF.

Sample name	Component A [wt%]	Component B [wt%]	Al [wt%]	CF [wt%]
SF	50	50	0	0
Al-SF(20 wt%)	40	40	20	0
Al-SF(40 wt%)	30	30	40	0
Al-SF(60 wt%)	20	20	60	0
CF-SF(20 wt%)	40	40	0	20
CF-SF(40 wt%)	30	30	0	40
CF-SF(60 wt%)	20	20	0	60
Al-CF-SF(60 wt%)	20	20	2	58

the SEM, the sample was cut into a small flat surface and fixing to the sample stage with a conductive adhesive, and sputtering gold was performed on the surface of the samples to increase the conductivity; the test voltage is 3 or 5 kV. X-ray diffraction (XRD) patterns were taken from a Rigaku diffractometer (D/Max 2500, Japan) with Cu K_{α} radiation ($\lambda = 0.154598$ nm) and scanned from 20° to 70° at a rate of $5^{\circ} \cdot \text{min}^{-1}$. Tensile and compression tests were obtained by an electronic universal testing machine (XJ830, Shanghai Xiangjie Testing Instruments Co., Ltd.). The elongation at break and tensile strength of silicone foam was characterized according to ASTM D412-98a. Dumbbell-shaped specimens with a narrow width of 1.3 mm were tested at room temperature at a tensile speed of $5 \text{ mm} \cdot \text{min}^{-1}$, and three parallel tests were performed for each group of specimens, and the average values were taken. Because the specimen is too thin, the compression test did not use the national standard, instead the sample was a small 30 mm diameter disc, and the loading rate was $1 \text{ mm} \cdot \text{min}^{-1}$. The thermal conductivity was tested by a heat flow method thermal conductivity instrument (DRL-V, Xiangtan Xiangyi Instruments Co. Ltd., Hunan, China). The infrared (IR) thermal images were captured by an IR camera (HIKMICRO, H11, China). Thermogravimetric analysis (TGA) was performed with a TGA 209F3A (NETZSCH, Germany) in the range of 40 to 800°C at a $10^{\circ}\text{C} \cdot \text{min}^{-1}$ heating rate under an air atmosphere. Fourier transform infrared spectrometer (Perkin Elmer, America) can obtain spectra with a resolution of 0.5 cm^{-1} in the wave number range of 4000 to 400 cm^{-1} . We use a

$100 \times 100 \times 1$ mm sheet for the voltage breakdown test (Jilin Feng Yuan Precision Electronic Equipment Co., Ltd., China).

2.4. Finite element simulation experiment

The simulations were modeled in two dimensions using SEM images as a reference in a $200 \times 150 \mu\text{m}$ area of the matrix. Silicone is the matrix, and circles of different diameters represent similarly sized aluminum spheres that are randomly distributed in the matrix. Rectangles of different sizes represent CF, which is anisotropically distributed within the matrix, and ellipses represent vesicles produced by foaming. For transient heat transfer analysis, a constant temperature of 353.15 K was set at the lower boundary, and an ambient temperature of 298.15 K was set at the upper boundary, the left and right boundaries were designated as insulating boundaries, and the vesicles were set to radiate from the surface to the ambient.

3. Results and discussion

3.1. Microstructure of the composite materials

The specific preparation scheme is shown in Figure 1. Component A containing Si–OH bond with component B containing Si–H bond can crosslink together and produce hydrogen gas (H_2) in the presence of catalysts. The reaction occurs at 30°C for foaming, the generated H_2 acts as foaming agent, and therefore the production process is simple and clean. CF and Al powder are both high thermally conductive fillers; they can be evenly dispersed within the silicone oil matrix. After mixing, they are evenly spread

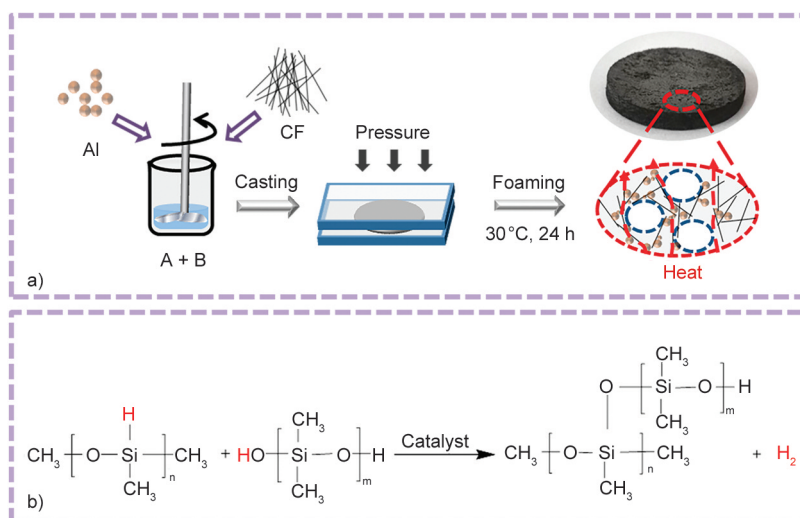


Figure 1. a) Preparation scheme of silicone foam with heat transfer network, b) foam generation mechanism.

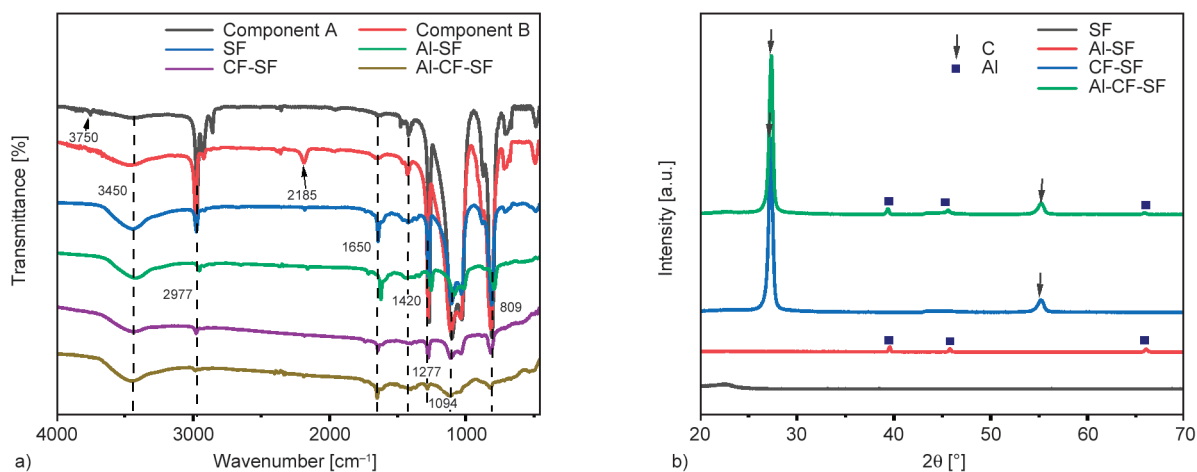


Figure 2. a) Fourier transform infrared spectrum of matrix and SF. b) The XRD patterns of SF, Al-SF, CF-SF and Al-CF-SF.

on the glass plate and a certain pressure is applied, which can control the foam thickness. The K of SF composites can be improved by forming thermal conductive paths inside the composites so that the excess heat can be dissipated.

Figure 2a shows the IR spectra of silicone oil A/B and SF. The peak at 3450 cm^{-1} is the absorption of the O–H group, which comes from H_2O in KBr. The peaks at 2977 and 1277 cm^{-1} are the absorption of Si–CH₃ stretching and bending vibrations, respectively. The peak at 1650 and 1420 cm^{-1} corresponds to the expansion vibration of CH₂=CH₂. The peaks at 1094 cm^{-1} are the Si–O–Si group of the coupling agent. The peak at 809 cm^{-1} is the stretching vibrations of the –CH=CH₂ and Si–CH₃ groups [25]. The peak at 3750 cm^{-1} in component A is the absorption of Si–OH deformation vibrations. The peak at 2185 cm^{-1} in component B is the absorption of the Si–H group. As can be seen from the figure, the peaks at 3750 and 2185 cm^{-1} disappear after the synthesis of SF, indicating that components A and B were successfully crosslinked. In addition, after adding the filler Al spheres and CF, the infrared spectrum of SF did not produce new peaks, indicating that there is only physical mixing between the filler and the SF without chemical reaction.

The crystal structure analysis of the composites was performed and the XRD spectra is shown in Figure 2b. The peaks observed at 26.3° and 54.1° are the diffraction peaks corresponding to carbon with the corresponding crystal planes (002) and (004). The peaks observed at 38.4° , 44.7° , and 65.1° are the diffraction peaks corresponding to Al spheres with corresponding crystal planes (111), (200), and (220). With the

increase of CF content, the higher the intensity of the diffraction peak of carbon peak, the amount of Al spheres in the Al-CF-SF is very little, so the intensity of the diffraction peak is weak.

Without any fillers, pristine SF dispersed a soft and transparent appearance (Figure 3). A large number of closed cells with an average diameter of $500\text{--}1500\text{ }\mu\text{m}$ were formed in SEM images, and the wall thickness is around $150\text{ }\mu\text{m}$ between the vesicles.

Al spheres with the size of 5 , 10 , and $30\text{ }\mu\text{m}$ were used as fillers to investigate the effect of particle size on the cellular size, and thermal and mechanical properties. After being filled with Al particles, the hybrid Al-SF appears gray (Figure 4). From the SEM images of $5\text{ }\mu\text{m}$ Al particles filled SF (Al-SF) in Figure 4, it can be seen that the Al spheres are uniformly dispersed in the matrix. When the filling amount of Al sphere is $20\text{ wt}\%$, the size of the bubble pore is about $650\text{ }\mu\text{m}$; as the filling amount of Al spheres increases, the bubble pores are destroyed, and the size decreases. With the filling amount of $40\text{ wt}\%$, the pore size is about $350\text{ }\mu\text{m}$, and with the filling amount of $60\text{ wt}\%$, the pore size is about $230\text{ }\mu\text{m}$. It can be seen that the increase in the number of Al spheres makes the bubble holes get destroyed, and the bad conductor of heat is reduced, which is conducive to the formation of thermal conductivity paths.

When filled with $10\text{ }\mu\text{m}$ Al spheres, the foam size of Al-SF was $400\text{ }\mu\text{m}$ at $20\text{ wt}\%$ filling, which was $200\text{ }\mu\text{m}$ smaller than $5\text{ }\mu\text{m}$ filled Al-SF, and the cell sizes were reduced by 70 and $20\text{ }\mu\text{m}$ at 40 and $60\text{ wt}\%$ filling, respectively (Figure 5).

The SEM images of $30\text{ }\mu\text{m}$ Al particles filled Al-SF composite are shown in Figure 6. When the filling

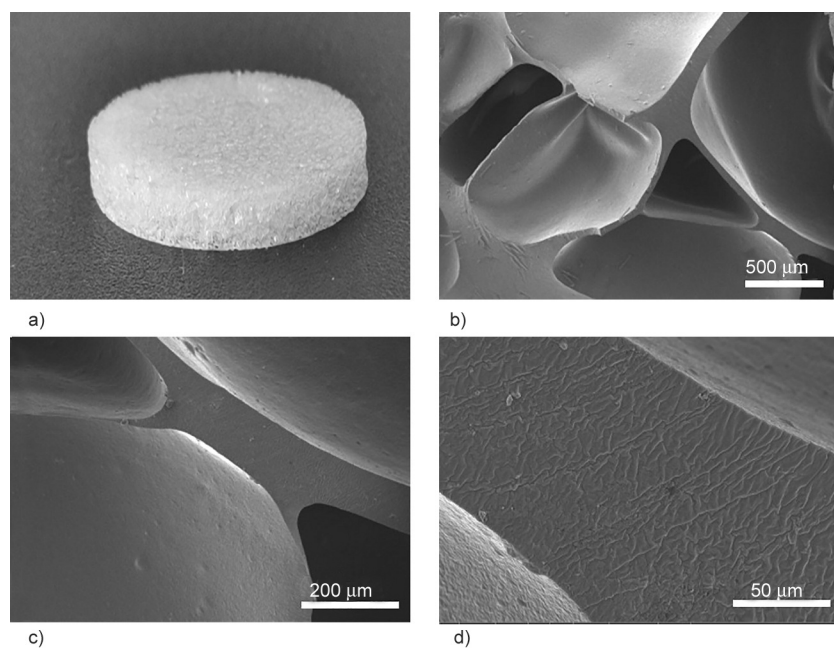


Figure 3. a) The appearance ($d = 30$ mm) and SEM images at b) 150 \times , c) 500 \times , d) 2000 \times of pristine SF.

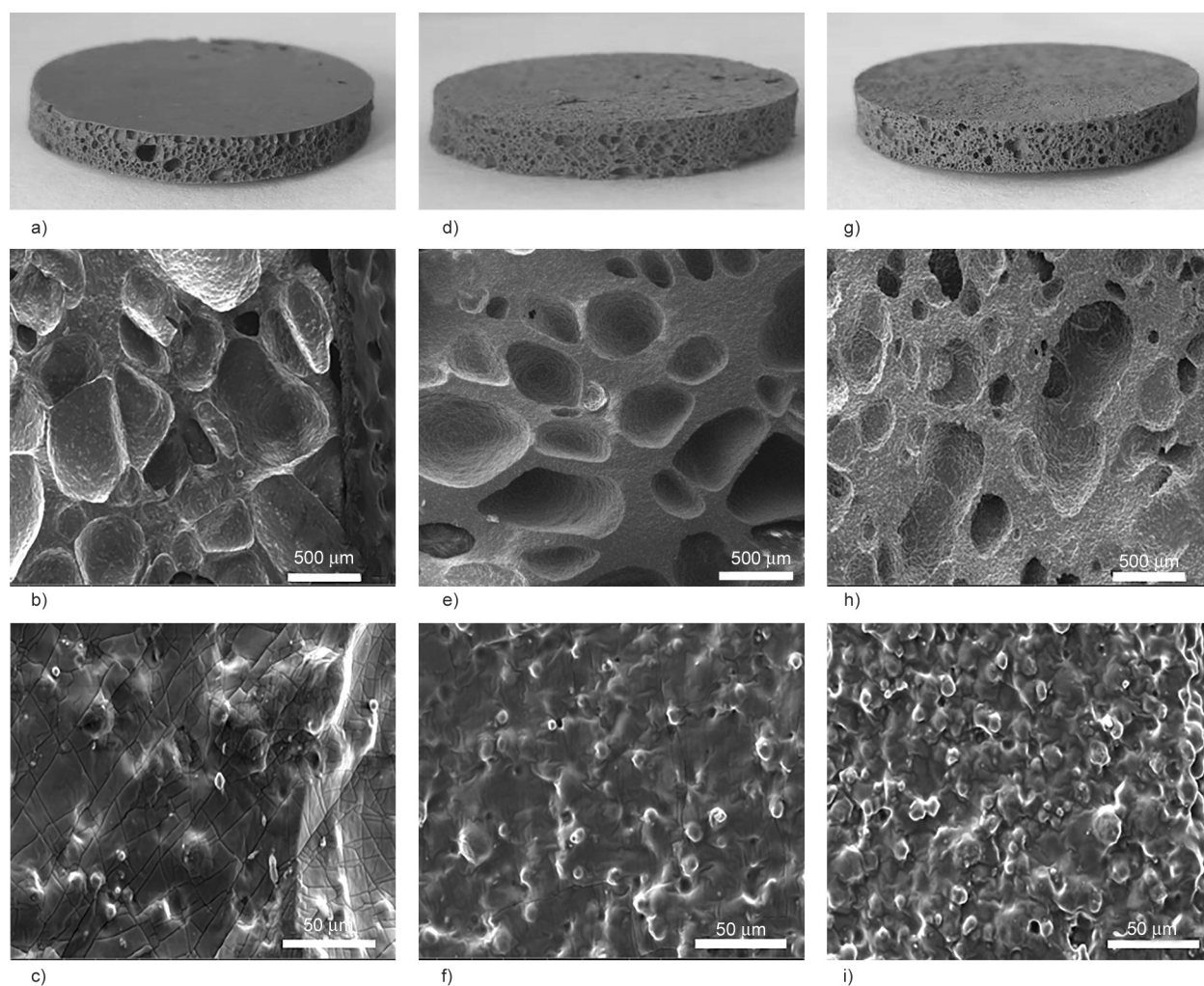


Figure 4. Morphology of 5 μm Al particles filled sample (Al-SF), Al with 20 wt% filling: a) appearance ($d = 30$ mm), SEM at b) 150 \times and c) 2000 \times . Al with 40 wt% filling: d) appearance ($d = 30$ mm), SEM at e) 150 \times and f) 2000 \times . Al with 60 wt% filling: g) appearance ($d = 30$ mm), SEM at h) 150 \times and i) 2000 \times .

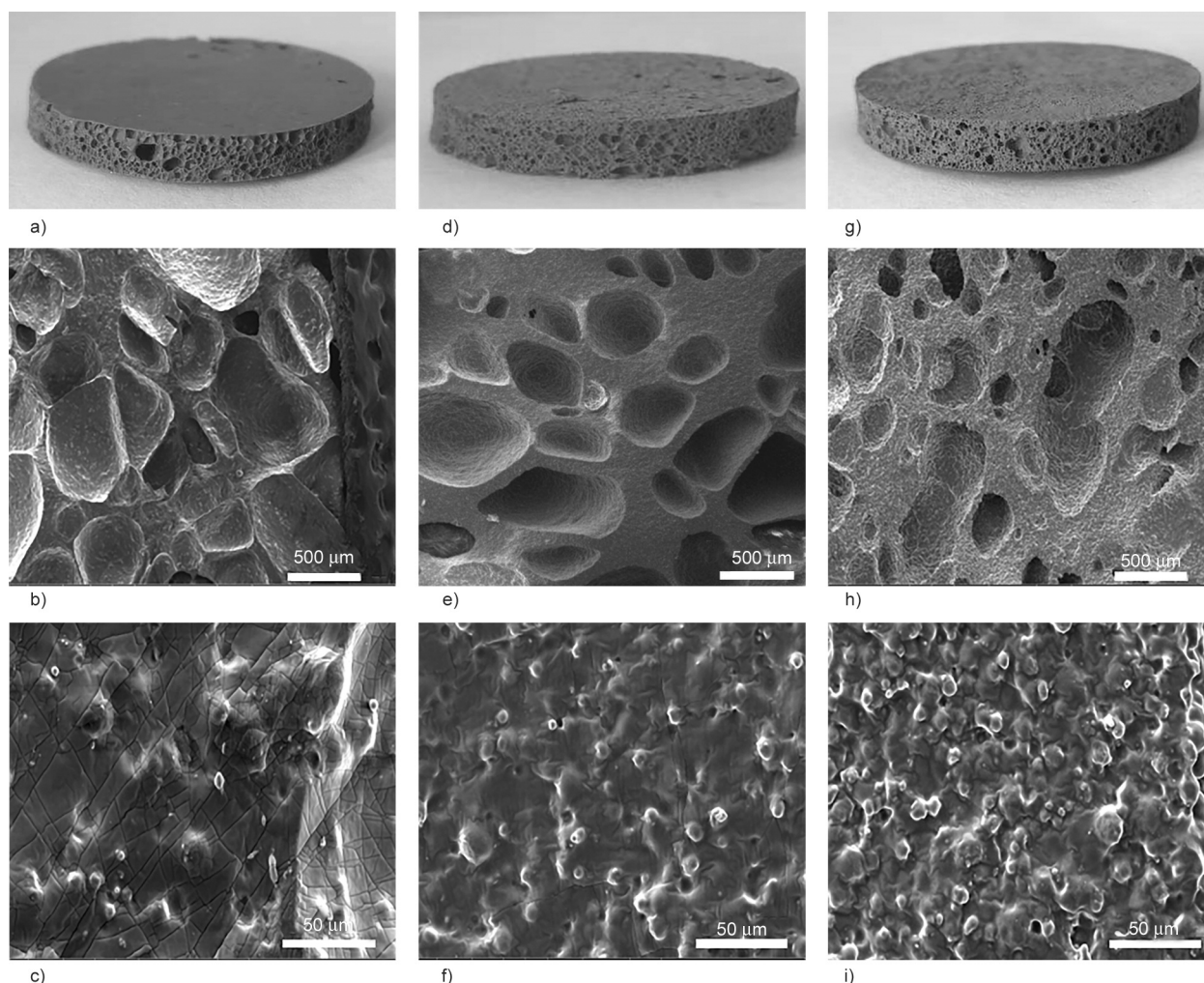


Figure 5. Morphology of 10 μm filled sample Al with 20 wt% filling: a) appearance ($d = 30\text{ mm}$), SEM at b) 150 \times and c) 2000 \times . Al with 40 wt%: filling d) appearance ($d = 30\text{ mm}$), SEM at e) 150 \times and f) 2000 \times . Al with 60 wt%: filling g) appearance ($d = 30\text{ mm}$), SEM at h) 150 \times and i) 2000 \times .

amount was 20 wt%, the size of vesicles was 350 μm and open pores with a size of 100 μm started to appear. Under the same filling amount, 30 μm Al spheres can occupy more voids between the bubble pores, which can preferentially form a thermally conductive network with low interfacial thermal resistance, and can effectively improve the thermal conductivity of the composite [26].

CF with higher K along its fiber direction is further used as fillers to prepare the hybrid SF. Figure 7 is the SEM photograph of CF-SF, from which it can be seen that CF is randomly distributed in the matrix at different angles, and some CF are connected with each other. CF-SF is almost always open-pore; with the increase of the filling amount, the size of the opening gets bigger and bigger; when the filling amount is 60 wt%, the filling amount inside the material tends to be saturated, and there is almost no

extra void, so it is difficult to continue to increase the thermal conductivity filler.

In order to construct a more effective heat transfer network, we adopt a combination of point and line methods to hybridize Al spheres and CF to obtain more excellent thermal conductivity. Figure 8 shows the microstructure of the Al-CF-SF at 60 wt% filling; SEM images show the uniform dispersion of CF and Al spheres in the silicone rubber matrix with good compatibility, which can effectively improve thermal conductivity. As can be seen from the energy dispersive spectroscopy (EDS) image, CF occupies a large number of voids; Al spheres can fill small voids to form a more compact heat transport network. The morphology of CF is a one-dimensional rod, represented as a long rectangle in Figure 8e, so we can determine the position of CF by comparing the morphology of the C element. The PDMS is mainly

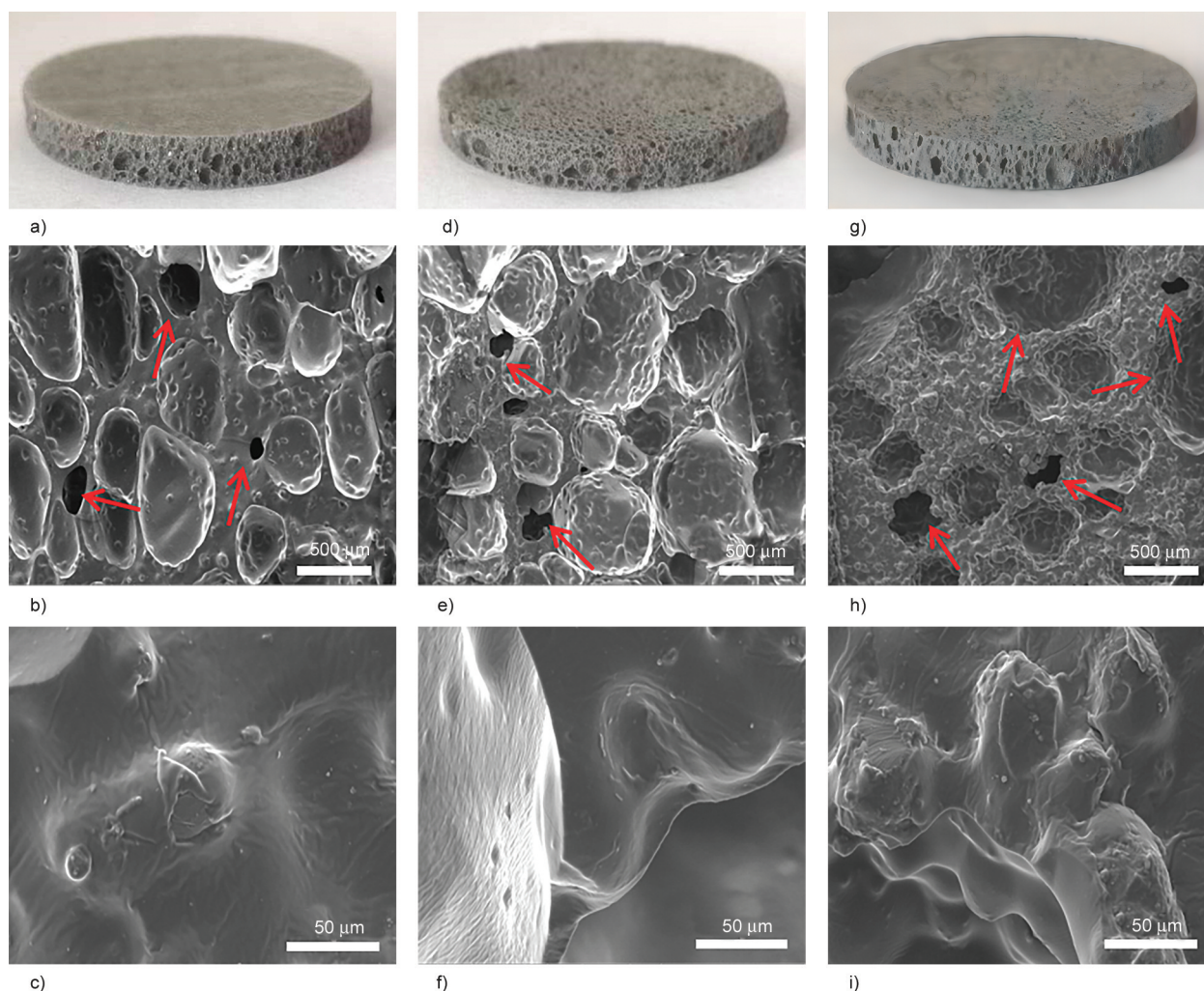


Figure 6. Morphology of 30 μm filled sample, Al with 20 wt% filling: a) appearance ($d = 30\text{ mm}$), SEM at b) 150 \times and c) 2000 \times . Al with 40 wt% filling: d) appearance ($d = 30\text{ mm}$), SEM at e) 150 \times and f) 2000 \times . Al with 60 wt% filling: g) appearance ($d = 30\text{ mm}$), SEM at h) 150 \times and i) 2000 \times .

composed of Si, O and C for rubber. The Si element has a large relative atomic mass and a strong signal, which makes it easy to determine the distribution of the PDMS, so the position of C in the matrix can also be determined from the position of Si. There is almost no air inside the composite material, the volume of the formed vesicles is extremely small, almost open pores, forming a filler synergistic heat transfer network mechanism which has a great improvement on the thermal conductivity.

3.2. Breakdown voltage of composites

The variation curves of the breakdown strength of Al-SF, CF-SF and Al-CF-SF with different filler levels are shown in Figure 9. It can be seen that the breakdown voltage strength of SF decreases with the increase of filling amount, and the dielectric strength decreases from 2.23 to 0.25 $\text{kV}\cdot\text{mm}^{-1}$ when

adding CF of 60 wt%. The 5 μm Al, 10 μm Al, and 30 μm Al filled silicon foams also decrease by 2, 3.6, and 2.8 $\text{kV}\cdot\text{mm}^{-1}$, respectively. This is due to the more filler content, the poorer the dispersion in the matrix agglomeration phenomenon is more obvious, the defects of the silicon foam increase, the charge aggregation occurs the more prone to breakdown. In addition to this, the addition of filler introduces more starting electrons, which is easier to move, and as the electrons collide with each other more electrons are produced, and the breakdown voltage strength is therefore reduced.

3.3. Mechanical properties of composites

3.3.1. Compressive properties of composites

Silicone rubber foams are highly elastic materials with compression capability, so the study of compression properties is an important indicator of the

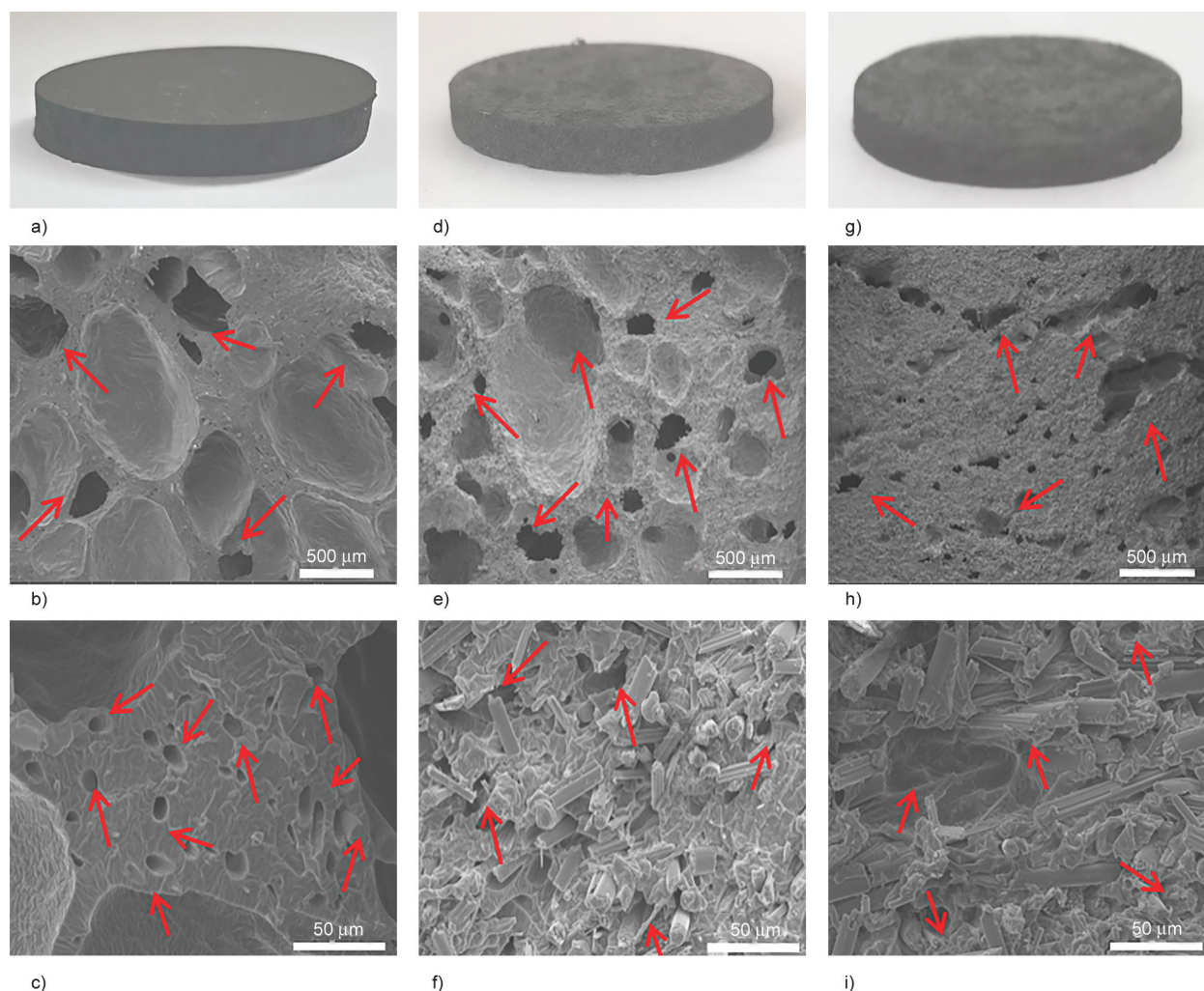


Figure 7. Morphology of CF-SF, CF with 20 wt% filling: a) appearance ($d = 30$ mm), SEM at b) 150 \times and c) 2000 \times . CF with 40 wt% filling: d) appearance ($d = 30$ mm), SEM at e) 150 \times and f) 2000 \times . CF with 60 wt% filling: g) appearance ($d = 30$ mm), SEM at h) 150 \times and i) 2000 \times .

response of foams to strain rates [27]. Figure 10 shows the stress-strain graphs and compression modulus of silicone rubber foam composites with different fillers. It can be seen that the incorporation of Al spheres and CF significantly increased the stress and modulus of the composites, where the 60 wt% CF-SF had the highest compressive stress of 1.34 MPa and compressive modulus of 3.36 MPa at a compressive strain of 40%, which were higher than those of the pure SF by 1.3 and 3.26 MPa, respectively. At low filling levels the foam is soft, and the particles are individually distributed in the composite matrix, making it difficult to form a continuous network. At this time, most of the pores in the foam material are closed and contain a large amount of gas inside. When the pore wall and the internal gas are subjected to part of the pressure, the pore collapses, then the gas quickly overflows outward, and

a very small pressure value can make the foam material produce a large deformation. However, when the foam material with 60 wt% filler is deformed by external force, the interaction between particles will hinder molecular movement, and the hardness of the composite material will become large and difficult to deform. It is noted that Al-CF-SF is hard to compress with a high compress ratio. Under the same testing condition, the compress stress is 0.5 MPa (a strain of 10%) and 2.0 MPa (a strain of 20%), respectively. A larger compression ratio would be beyond the test range of the instrument (2 MPa).

3.3.2. Tensile properties of composites

Tensile properties are an important indicator that characterizes the resistance of the foam to elastic deformation under the action of external forces. Figure 11 shows the tensile stress-strain curves of CF and Al

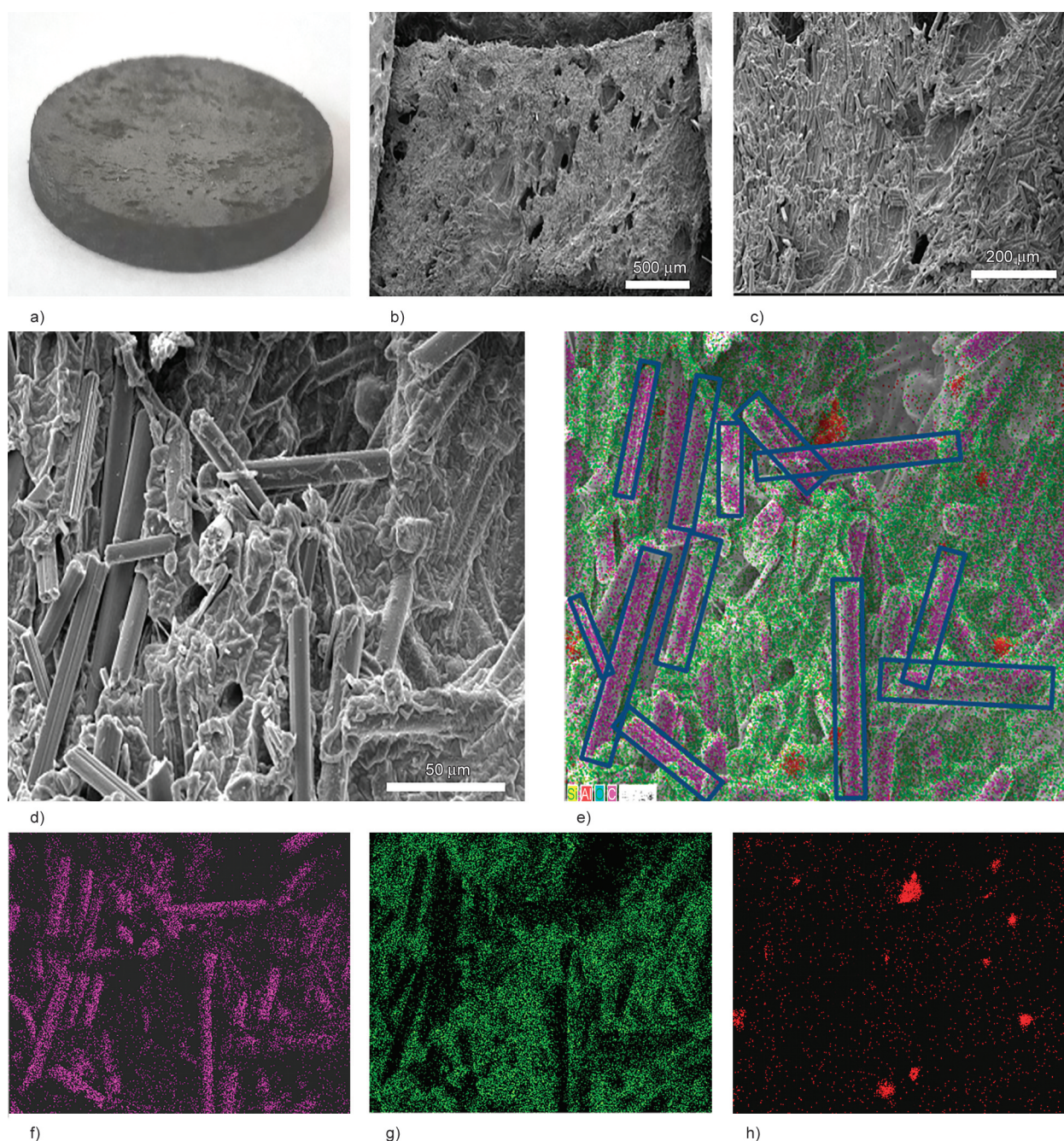


Figure 8. Morphology of Al-CF-SF: a) appearance ($d = 30$ mm). SEM at b) 150 \times , c) 500 \times , d) 2000 \times . e) EDS at 2000 \times , elements mapping of f) C, g) Si, and h) Al.

spheres filled alone and mix filling of Al-CF-SF. It can be seen that pure SF requires only 0.1 MPa of stress to achieve 105% strain and has good elasticity. With the increase of the filling amount the stress gradually becomes larger, and the strain becomes smaller, indicating that the addition of filler makes the SF harder and more difficult to deform. 60 wt% CF-SF has the highest stress of 0.72 MPa, but only 6% deformation.

Tensile strength is the maximum stress that a material can withstand during the stretching process and

it can be seen that the tensile strength and tensile modulus of the composite increases with the increase of the filler amount. The increase in the amount of filler facilitates the formation of a tight crosslinked network of SF, which increases the hardness and requires more force in tension and increases the tensile strength. For the tensile strength of Al-SF with different particle sizes, 5 μm Al > 10 μm Al > 30 μm Al. It is possible that this is due to the greater number of small particle size fillers at a given weight of filling and the greater contact area with the matrix. When

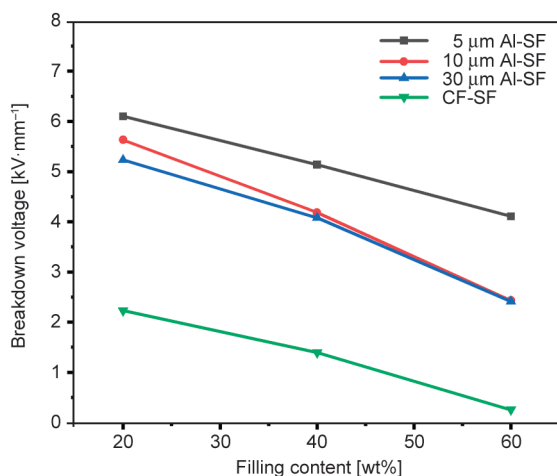


Figure 9. Variation of breakdown strength of prepared silicone rubber foam composites with different filling content.

the filling amount is 60 wt%, the tensile strength and tensile modulus of 30 μm Al-SF is the minimum of 0.24 and 0.86 MPa, respectively, and the maximum of CF-SF is 0.72 and 10.86 MPa, respectively.

Fracture strain is the maximum strain to which the material is subjected before fracture. The trend of the fracture strain of SF is the opposite of the tensile strength, which gradually decreases with the increase of the filling amount. It may be due to the formation of stress concentration points by restricting the movement of molecular chains when filling Al spheres and CF in the matrix. These stress concentration points increase when the filler content increases, making the composites susceptible to fracture when subjected to external forces, which decreases the fracture strain. The material does not yield at fracture and is brittle with poor fracture toughness.

3.4. Thermal properties of composite materials

3.4.1. Effect of filler on thermal conductivity

To explore the relationship between K and filler distribution, the K of the composites was measured by the heat flow method. The K of the composite was measured at 70 °C using different pressures (50 N/100 N/150 N/200 N/250 N/300 N). The thermal conductivity of the filler itself and its filling amount and distribution in the silicon matrix affect the overall thermal conductivity of the composite. Different particle sizes of fillers have different distributions in silicone rubber, and at a certain amount

of filling, it can be seen from Figure 12a that the K sizes corresponding to different particle sizes of fillers are: 30 μm Al > 10 μm Al > 5 μm Al. Since the Al spheres are small, the particles cannot contact each other and do not form a complete thermal conductivity network chain within the matrix; the thermal conductivity of the composites formed by different particle size Al spheres is not significantly enhanced. CF has a high thermal conductivity and aspect ratio compared to Al spheres, making it easier to form a thermal conductivity network. Therefore, the highest thermal conductivity of 1.2 W·m⁻¹·K⁻¹ was achieved for CF with 60 wt% filling at 300 N, which is more than five times higher than the thermal conductivity of Al-SF composite.

The change of filling amount also affects the thermal conductivity of the composite. Taking 5 μm Al spheres as an example, when the filling amount is small, the particles are uniformly dispersed in the silica matrix without contacting with each other, which may lead to a larger thermal resistance and low thermal conductivity. But with the increase of thermally conductive filler, Al spheres began to have contact, the thermal conductivity network chain gradually improved, the thermal conductivity increased rapidly. But when the Al spheres increased to a certain extent, the formation of the overall thermal conductivity network structure, reached the maximum filling volume, continue to increase the amount of filler, the filler will disperse the matrix outside can not be completely surrounded. In this experiment, the composite reached the critical filling amount when the filling amount was 60 wt%, and it was more difficult to mix. In addition, carbon fibers are one-dimensional columnar structures, the effective connection between carbon fibers is limited, and the ability to participate in phonon transport directly is poor, resulting in high interface thermal resistance.

In order to optimize the thermal conductivity of the composite material, we fix the maximum filling amount of the composite material to 60 wt%, based on which the CF and Al spheres are compounded because the CF can improve the thermal conductivity of the composite material more effectively, we use a small percentage adjustment to replace the CF with Al spheres. Al spheres can fill the gaps between CF and increase site contact. The thermal conductivity of CF compounded with different particle sizes of Al spheres is shown in Figure 12b, from which it

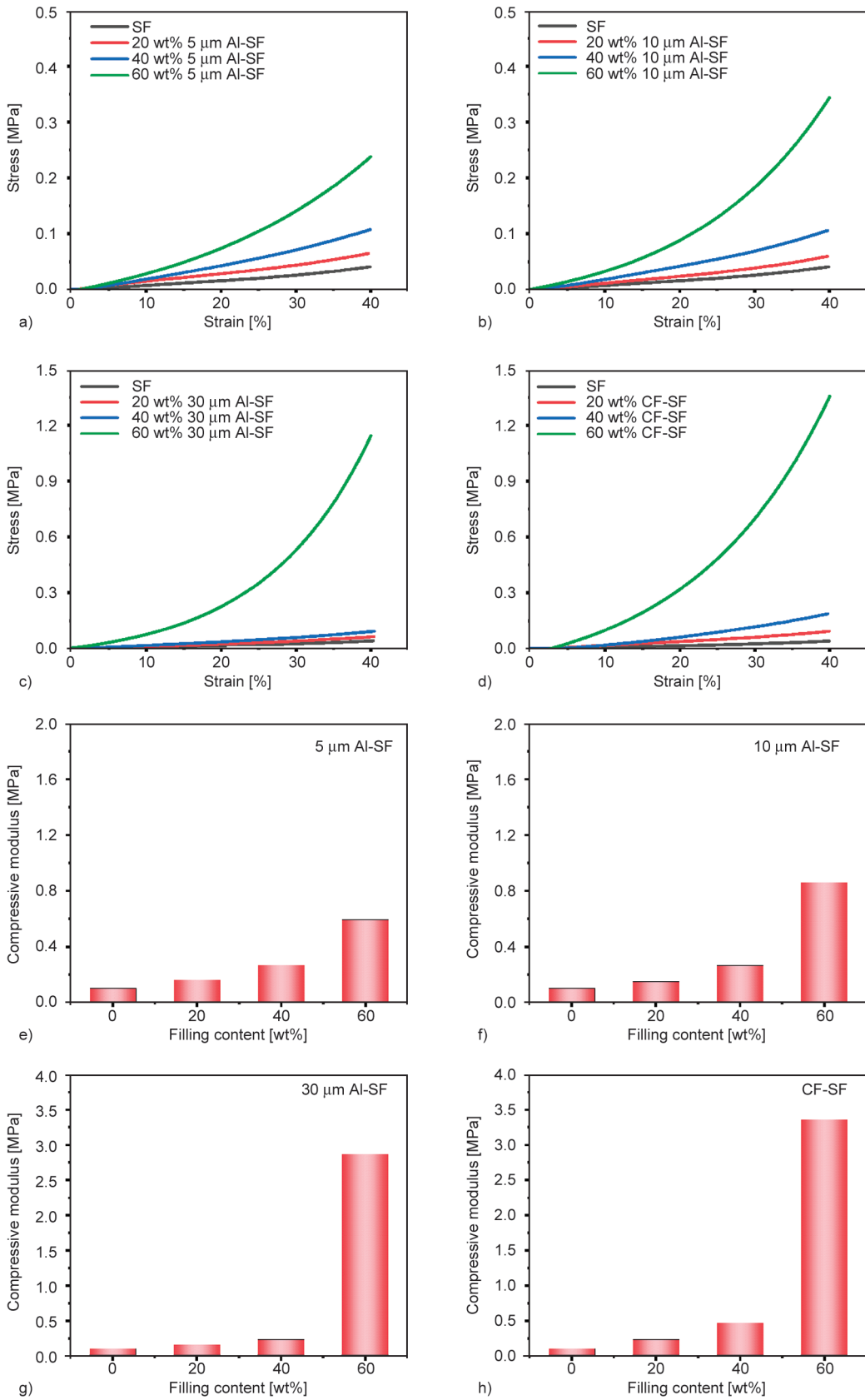


Figure 10. Compressive stress-strain curves for composites filled with different fillers a) 5 μm Al, b) 10 μm Al, c) 30 μm Al, d) CF. Compressive modulus curves for composites filled with different fillers e) 5 μm Al, f) 10 μm Al, g) 30 μm Al, h) CF.

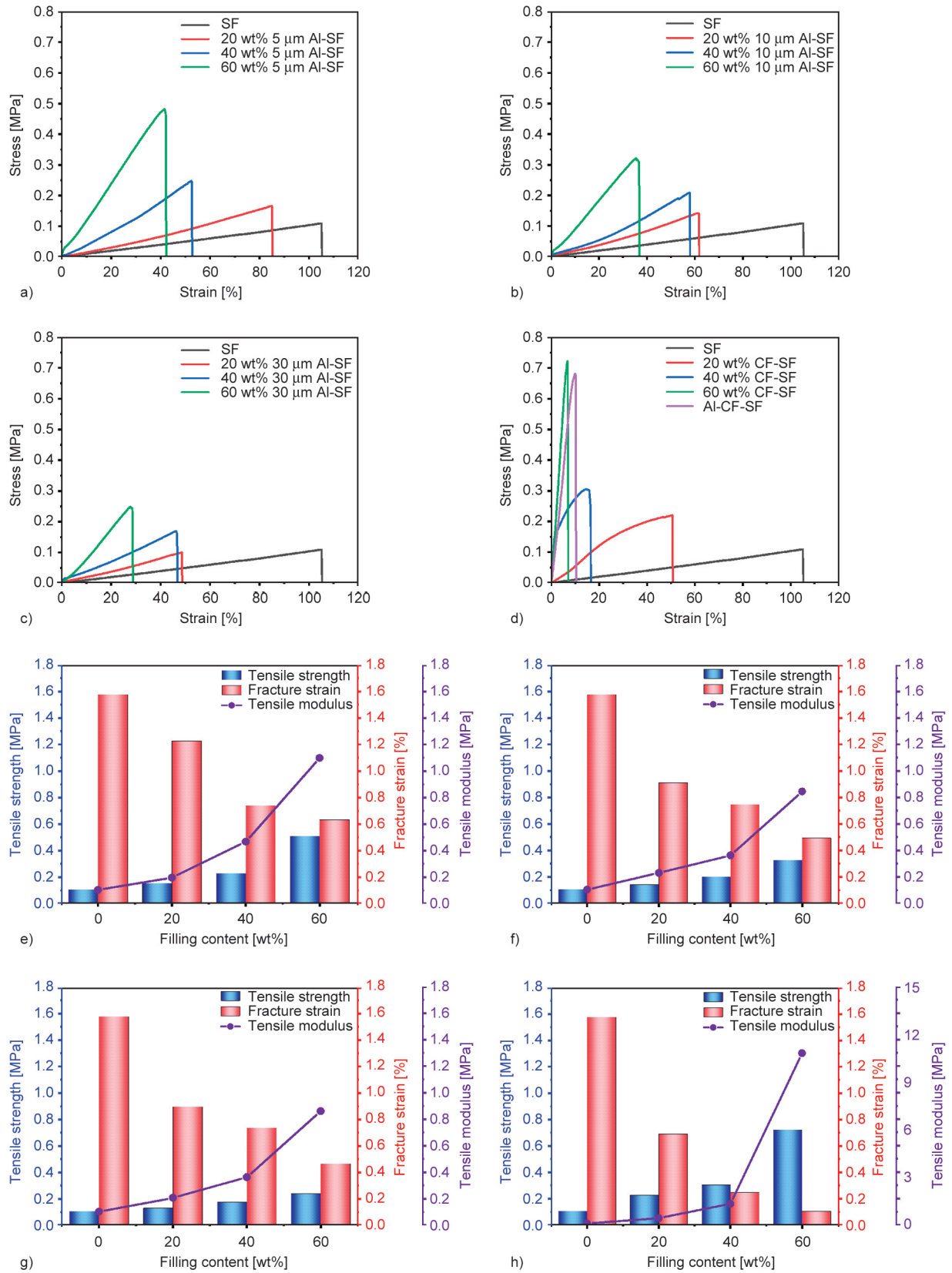


Figure 11. Tensile stress-strain curves for composites filled with different fillers a) 5 μm Al, b) 10 μm Al, c) 30 μm Al, d) CF. Variation of tensile strength, modulus and fractures strain with filler content e) 5 μm Al, f) 10 μm Al, g) 30 μm Al, h) CF.

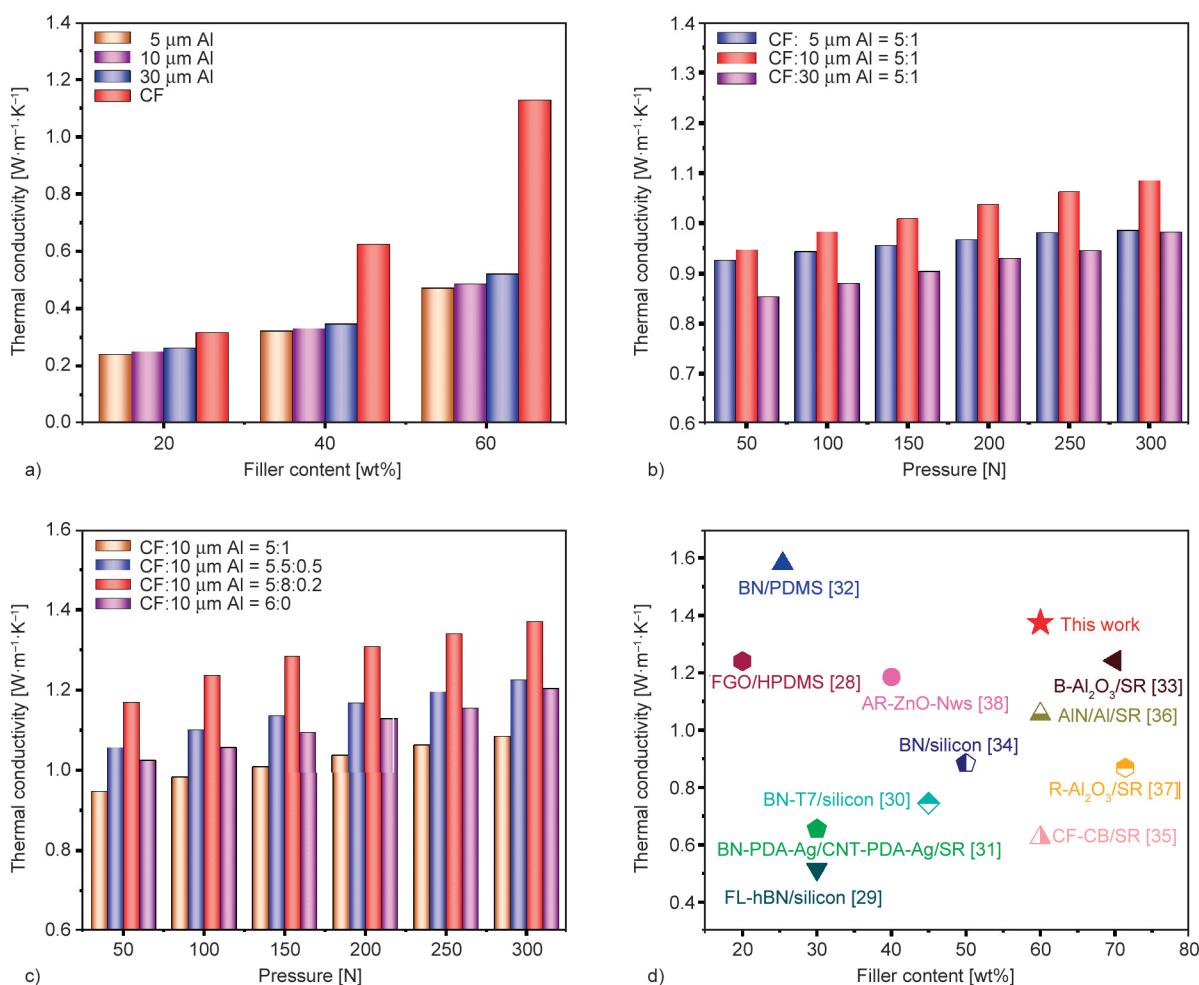


Figure 12. Thermal conductivity of a) SF composites formed by different fillers, b) compounding of CF and Al of different particle sizes, c) compounding of CF and 10 μm Al at different filler ratios, d) comparison of this work with previous studies.

can be seen that the thermal conductivity of carbon fiber compounded with 10 μm Al spheres is higher than that with the other two particle sizes, and the thermal conductivity is $1.08 \text{ W}\cdot\text{m}^{-1}\cdot\text{K}^{-1}$ at 300 N pressure. Therefore, we investigated the effect of the compounding ratio on the thermal conductivity of the composites by changing the compounding ratio of carbon fiber to 10 μm Al spheres. As shown in Figure 12c, the thermal conductivity of the composites reached a maximum value of $1.37 \text{ W}\cdot\text{m}^{-1}\cdot\text{K}^{-1}$, when the filler ratio CF:10 μm Al = 5.8:0.2, which is 9.7 times higher than that of the pure silica matrix. Figure 12d shows the effect of thermally conductive fillers on the thermal properties of silicone composites, and by comparing it with the results of previous studies, it shows that this experiment effectively constructs a dense and efficient thermal conductivity network [28–38].

3.4.2. Finite element model of SF composites

In order to explain the thermal conductivity mechanism of the composites in more depth we performed simulations using finite element analysis. We have created three simulations for single filler (Al-SF, CF-SF) and mixed filler (Al-CF-SF) as shown in Figure 13. The simulation results proved that the hybrid filler had a faster heat transfer rate than the single filler. Al powder exists in the matrix in point form and it is difficult to contact between particles, which mainly depends on the heat transfer of the matrix. CF is arranged in the matrix in a linear form, which increases the possibility of contact with each other, but it also hampers the improvement of the thermal conductivity because of the limited space inside the matrix. When CF and Al powder are added to the matrix in a certain ratio, the internal space of the matrix can be fully utilized, and the carbon fiber can

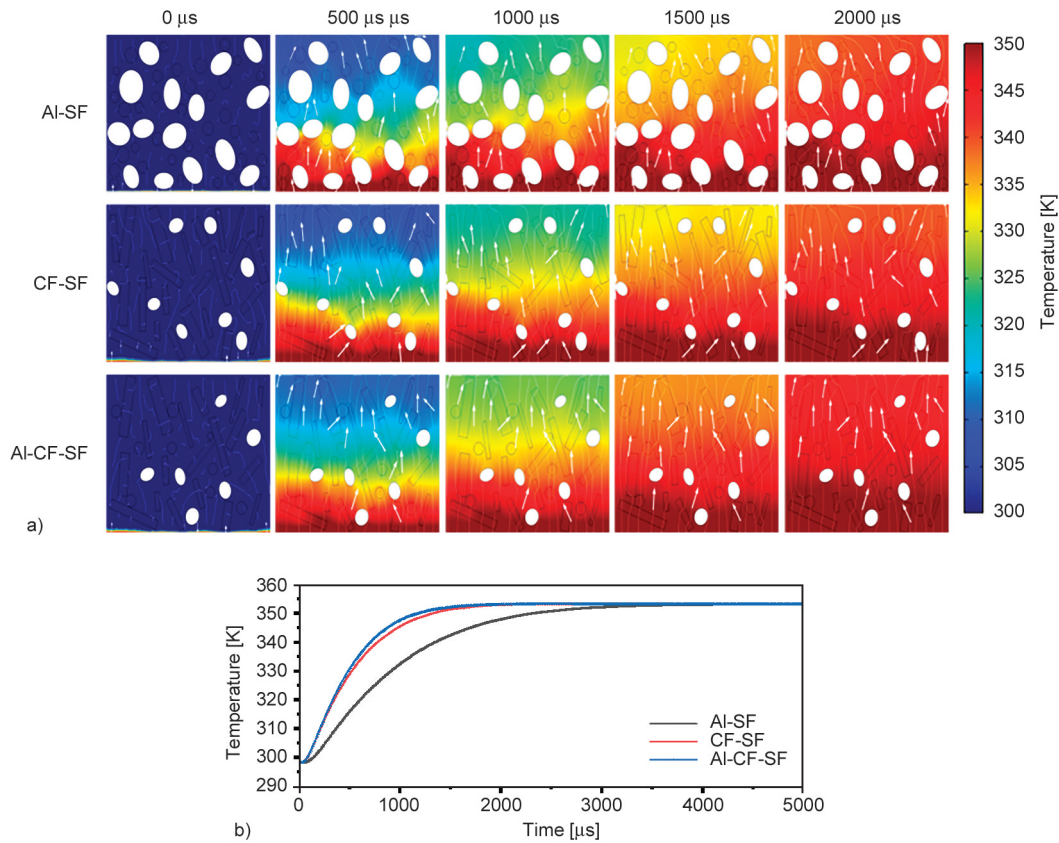


Figure 13. The finite element analysis results of Al-SF, CF-SF, and Al-CF-SF a) temperature distribution and heat flux direction modeling, white flow lines, and arrows indicate the heat flux and the direction of heat flux, respectively, b) time-temperature profile.

form a long-distance thermal conductivity pathway, while the Al powder plays the role of a bridge connecting the pathways, forming a ‘point and line synergistic’ thermal conductivity network conductivity mode inside the matrix.

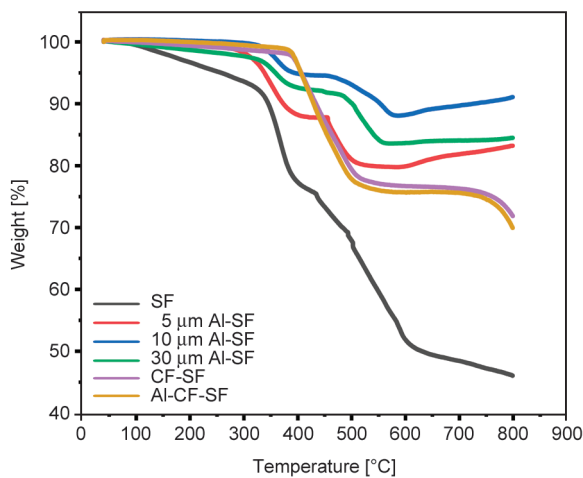


Figure 14. The weight loss curves of silicone foam composite.

3.4.3. Stability of the composites

The thermal stability is a measure of the ease of thermal decomposition of the sample, the thermal weight loss behavior of the silica foam composite filled with 60 wt% under an O₂ atmosphere is shown in Figure 14. The results showed that the temperature of 5% weight loss of these composites occurred at 246 °C (SF), 338 °C (5 μm Al-SF), 358 °C (10 μm Al-SF), 391 °C (30 μm Al-SF) and 405 °C (CF-SF, Al-CF-SF). At 600 °C, the weight loss of SF, 5 μm Al-SF, 10 μm Al-SF, 30 μm Al-SF, CF-SF, and Al-CF-SF were 49, 21, 12, 17, 24 and 25%, respectively. It can be seen that the weight loss of the composites after the addition of fillers is significantly lower than that of the pure SF, and the thermal stability is better.

In the actual work condition, the performance of foam has kept stability undergoing multiple compresses. To calculate the mechanical dissipation loss of stress-strain, we did the compression-release cycle test and measured the thermal conductivity every

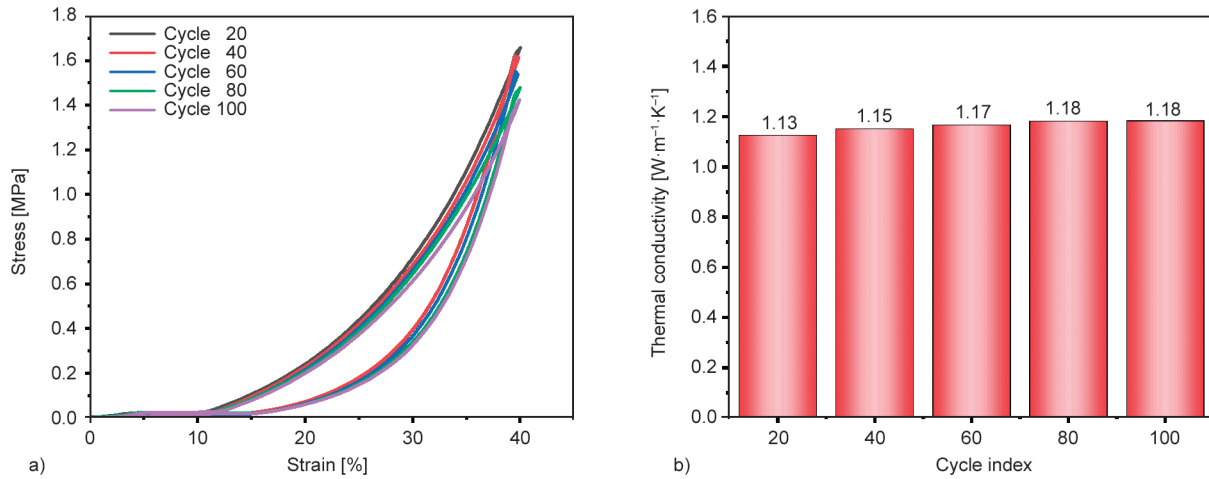


Figure 15. a) Stress-strain curve of CF-SF during compression-release cycle process. b) The thermal conductivity of CF-SF was measured every 20 cycles.

twenty cycles from CF-SF (60 wt%) [39]. The cycle test curve of CF-SF with 60 wt% filler compression of 40% is shown in Figure 15a, and it can be found that the hysteresis returns a line of the foam material in the shape of a crescent and partially overlapped, which indicates that the CF-SF has undergone a relatively small energy loss in the cycling process. The dissipated energy was obtained from the area of the closed graph of the stress-strain curve, and it was found that the energy dissipation was 4.77 J at 100 cycles, which is a small amount of 2 J compared with the loss at the first cycle. At the same time, it can be

seen that the thermal conductivity corresponding to Figure 15b is slightly increased. The thermal conductivity of the sample before the start of the cycle is $1.05 \text{ W}\cdot\text{m}^{-1}\cdot\text{K}^{-1}$. After 100 cycles, the thermal conductivity is $1.18 \text{ W}\cdot\text{m}^{-1}\cdot\text{K}^{-1}$, which is an increase of $0.13 \text{ W}\cdot\text{m}^{-1}\cdot\text{K}^{-1}$. Therefore the mechanical loss of SF can improve its thermal conductivity.

3.4.4. Thermal management application of SF composites

To study the thermal management ability of silicone rubber foam materials, we record the surface

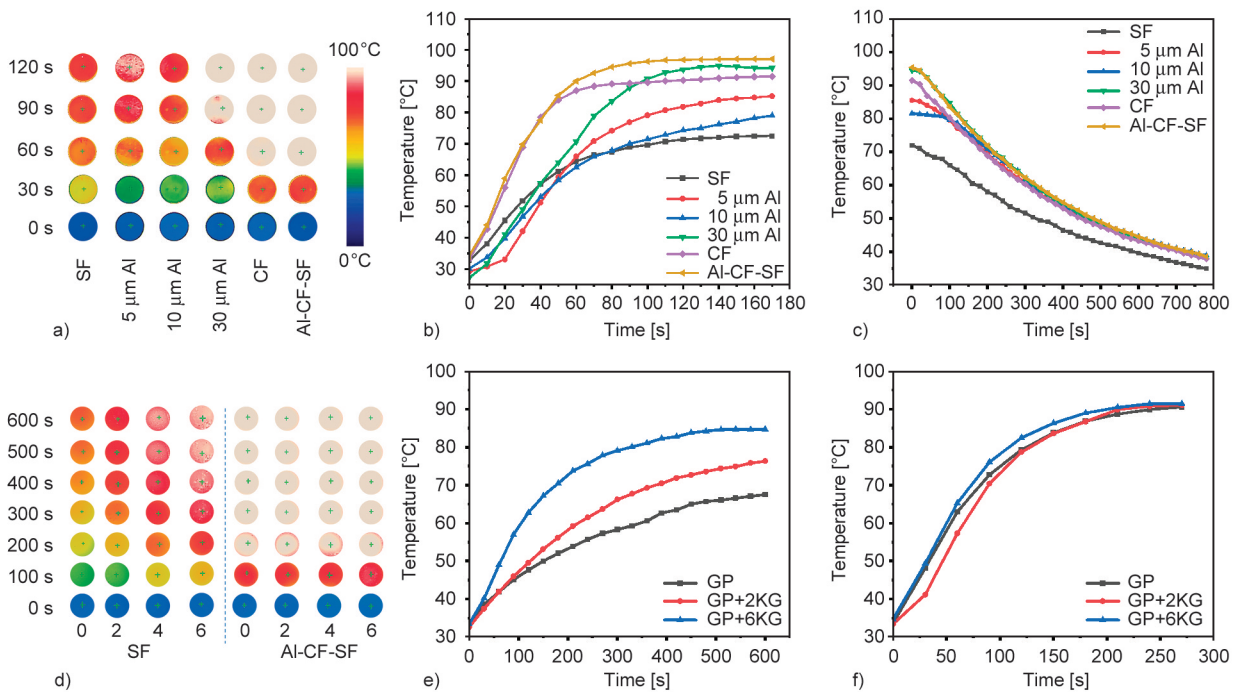


Figure 16. Surface temperature change of composites a) infrared thermal images, b) heating process and c) cooling process. After applying pressure d) infrared thermal images, heating up process of e) pure SF and f) Al-CF-SF.

temperature change of the sample with the help of the infrared camera. We placed the SF in the middle of a ceramic heating plate with a heating temperature range of 30–100 °C. The temperature change in the center of the sample was extracted every 30 s using an infrared thermographic camera, and the image of the sample surface temperature is shown in Figure 16a. Blue represents the lowest surface temperature of the sample; from the bottom to the top, the sample temperature gets higher and higher, and white represents the surface temperature of the sample that reaches above 90 °C. During the heating process, the color of the sample changes from dark to light, and the heat transfer rate becomes faster as time goes on. The images in Figures 16b and 16c represent the sample warming and cooling processes. The pure SF reached the heat transfer limit of 72 °C after heating for 170 s, while Al-CF-SF reached the sample surface temperature of 96 °C at 100 s, showing better thermal conductivity and heat dissipation during the heating and cooling processes.

In addition, to study the effect of pressure on the thermal conductivity of the foam, we placed a glass plate (GP) on the pure SF and Al-CF-SF and placed 0, 2, and 6 weights (one weight is 1 kg) on the glass plate to observe their thermal conductivity, respectively. The infrared thermography and heat transfer rates of the samples are shown in Figure 16d. We find from Figure 16e that the pressure has a greater effect on the thermal conductivity of pure SF, the heat transfer rate reaches equilibrium after heating 600 s. The highest heat transfer temperature of SF material with only glass plates placed is 68.3 °C, and the highest heat transfer temperature increases with the increase of the number of weights, and the highest heat transfer temperature of SF material with 6 weights placed can reach 84.5 °C which is 16.2 °C higher than that of pure SF. This is because the bubble pores are destroyed after applying pressure, which improves the heat transfer path inside the sample, and the heat transfer efficiency is greatly improved. However, as shown in Figure 16f, the effect of pressure on the Al-CF-SF is not obvious, and the temperature change tends to stabilize to 90 °C after 280 s, which is due to the that there are no voids inside the Al-CF-SF. The fillers are interconnected to form a complete crosslinked network.

4. Conclusions

In summary, we successfully synthesized silicone foam and hybrids by a simple process. A series of SF composites with highly efficient thermal conductive networks were designed and prepared by optimizing fillers' particle size and dimension. Observing the size of the vesicles inside the matrix by SEM demonstrated that incorporating fillers could exclude the excess air inside the matrix and thus improve thermal conductivity. The hybridized fillers made of Al particles and CF composite can occupy more voids to improve the thermal conductivity of the composites further. Infrared thermography and finite element modeling also further proved the accuracy of the experiments. Tensile and compressive characterization also demonstrated that the mechanical properties of the composites were improved compared to pure SF and that the loss of mechanical properties also contributed to the improvement of the material's thermal conductivity. Using a small amount of Al powder instead of CF in this study can reduce the cost and has great potential in the preparation of reinforced thermally conductive composites.

Acknowledgements

This work was supported by the Chinese National Natural Science Fund (12172118), the Research Program of Local Science and Technology Development under the Guidance of Central (216Z4402G) and the Foundation of State Key Laboratory of Coal Conversion of Shanxi Institute of Coal Chemistry, CAS (J22-23-610). Dr. Qibo Deng acknowledges support from the 'Yuanguang' Scholar Program of the Hebei University of Technology.

References

- [1] Rostami-Tapeh-Esmaeil E., Vahidifar A., Esmizadeh E., Rodrigue D.: Chemistry, processing, properties, and applications of rubber foams. *Polymers*, **13**, 1565 (2021). <https://doi.org/10.3390/polym13101565>
- [2] Duan Y., Chen X., Yin B., Zhao X., Zhao Z., Hou B., Li Y.: Understanding the effect of defects on compressive behaviors of closed-cell foams: Experiment and statistical model. *Composites Part B: Engineering*, **244**, 110179 (2022). <https://doi.org/10.1016/j.compositesb.2022.110179>
- [3] Peixinho N., Carvalho O., Areias C., Pinto P., Silva F.: Compressive properties and energy absorption of metal-polymer hybrid cellular structures. *Materials Science and Engineering: A*, **794**, 139921 (2020). <https://doi.org/10.1016/j.msea.2020.139921>

- [4] Yang J., Li P.: Characterization of short glass fiber reinforced polypropylene foam composites with the effect of compatibilizers: A comparison. *Journal of Reinforced Plastics and Composites*, **34**, 534–546 (2015).
<https://doi.org/10.1177/0731684415574142>
- [5] Yan H., Wang K., Zhao Y.: Fabrication of silicone rubber foam with tailored porous structures by supercritical CO₂. *Macromolecular Materials and Engineering*, **302**, 1600377 (2017).
<https://doi.org/10.1002/mame.201600377>
- [6] Abbad A., Jaboviste K., Ouisse M., Dauchez N.: Acoustic performances of silicone foams for sound absorption. *Journal of Cellular Plastics*, **54**, 651–670 (2017).
<https://doi.org/10.1177/0021955x17732305>
- [7] Grande J. B., Fawcett A. S., McLaughlin A. J., Gonzaga F., Bender T. P., Brook M. A.: Anhydrous formation of foamed silicone elastomers using the Piers-Rubinsztajn reaction. *Polymer*, **53**, 3135–3142 (2012).
<https://doi.org/10.1016/j.polymer.2012.05.033>
- [8] Yu Z., Ma L., Zhu B., Phule A. D., Wen S., Zhao Y., Zhang Z.: Development of EVA/POE/SEBS microcellular foam: Network structure, mechanics performance and midsole application. *Express Polymer Letters*, **16**, 1322–1330 (2022).
<https://doi.org/10.3144/expresspolymlett.2022.95>
- [9] Zhang C., Qu L., Wang Y., Xu T., Zhang C.: Thermal insulation and stability of polysiloxane foams containing hydroxyl-terminated polydimethylsiloxanes. *RSC Advances*, **8**, 9901–9909 (2018).
<https://doi.org/10.1039/c8ra00222c>
- [10] Wang X. J., Niu X. H., Wang X. X., Qiu X. W., Istikomah N., Wang L. B.: Thermal conductivity of porous polymer materials considering pore special-shape and anisotropy. *Express Polymer Letters*, **15**, 319–328 (2021).
<https://doi.org/10.3144/expresspolymlett.2021.28>
- [11] Lin X., Zhang X., Ji J., Liu L., Yang M., Zou L.: Experimental investigation of form-stable phase change material with enhanced thermal conductivity and thermal-induced flexibility for thermal management. *Applied Thermal Engineering*, **201**, 117762 (2022).
<https://doi.org/10.1016/j.applthermaleng.2021.117762>
- [12] Li P., Lan B., Zhang Q., Yang Q., Gong P., Park C. B., Li G.: Microcellular foams simultaneous reinforcing and toughening strategy of combining nano-fibrillation network and supercritical solid-state foaming. *Polymer*, **252**, 124928 (2022).
<https://doi.org/10.1016/j.polymer.2022.124928>
- [13] Li S. J., Li J. C., Ji P. Z., Zhang W. F., Lu Y. L., Zhang L. Q.: Bubble-templated construction of three-dimensional ceramic network for enhanced thermal conductivity of silicone rubber composites. *Chinese Journal of Polymer Science*, **39**, 789–795 (2021).
<https://doi.org/10.1007/s10118-021-2581-4>
- [14] Zhang Y.-L., Zang C.-G., Jiao Q.-J.: Electrical, thermal, and mechanical properties of silicone foam composites filled with carbon-based nanofillers. *Journal of Applied Polymer Science*, **137**, 49191 (2020).
<https://doi.org/10.1002/app.49191>
- [15] Shi S., Wang Y., Jiang T., Wu X., Tang B., Gao Y., Zhong N., Sun K., Zhao Y., Li W., Yu J.: Carbon fiber/phenolic composites with high thermal conductivity reinforced by a three-dimensional carbon fiber felt network structure. *ACS Omega*, **7**, 29433–29442 (2022).
<https://doi.org/10.1021/acsomega.2c03848>
- [16] Li H., Chen W., Xu J., Li J., Gan L., Chu X., Yao Y., He Y., Li B., Kang F., Du H.: Enhanced thermal conductivity by combined fillers in polymer composites. *Thermochimica Acta*, **676**, 198–204 (2019).
<https://doi.org/10.1016/j.tca.2019.04.008>
- [17] Zhang Y. L., Zang C. G., Jiao Q. J.: Electrical and thermal properties of silicone rubber composites filled with Cu-coated carbon fibres and functional carbon nanotubes. *Plastics Rubber and Composites*, **48**, 327–337 (2019).
<https://doi.org/10.1080/14658011.2019.1625249>
- [18] Wu Z., Xu C., Ma C., Liu Z., Cheng H.-M., Ren W.: Synergistic effect of aligned graphene nanosheets in graphene foam for high-performance thermally conductive composites. *Advanced Materials*, **31**, 1900199 (2019).
<https://doi.org/10.1002/adma.201900199>
- [19] Wang X., Liu H., Qiu X., Wang L., Wang L.: Thermal conductivity of filled composite materials considering interactions between fillers. *Applied Thermal Engineering*, **141**, 835–843 (2018).
<https://doi.org/10.1016/j.applthermaleng.2018.06.022>
- [20] Jiao T., Han B., Zhao L., Zhang Z., Zeng Y., Li D., Zhang K., Deng Q., Zhao Y., Li Z.: Pie-rolling-inspired construction of vertical carbon fiber high thermal conductivity hybrid networks. *Applied Surface Science*, **618**, 156711 (2023).
<https://doi.org/10.1016/j.apsusc.2023.156711>
- [21] Zhang P., Zeng J. H., Zhai S. P., Xian Y. Q., Yang D. G., Li Q.: Thermal properties of graphene filled polymer composite thermal interface materials. *Macromolecular Materials and Engineering*, **302**, 1700068 (2017).
<https://doi.org/10.1002/mame.201700068>
- [22] Smorygo O., Mikutski V., Marukovich A., Sadykov V., Bepalko Y., Stefan A., Pelin C.-E.: Preparation and characterization of open-cell epoxy foams modified with carbon fibers and aluminum powder. *Composite Structures*, **202**, 917–923 (2018).
<https://doi.org/10.1016/j.compstruct.2018.04.063>
- [23] Meng Z., Dai Z., Chen K., Wang S.: Investigation on preparation, thermal, and mechanical properties of carbon fiber decorated with hexagonal boron nitride/silicone rubber composites for battery thermal management. *International Journal of Energy Research*, **45**, 4396–4409 (2021).
<https://doi.org/10.1002/er.6110>

- [24] Wei J., Liao M., Ma A., Chen Y., Duan Z., Hou X., Li M., Jiang N., Yu J.: Enhanced thermal conductivity of polydimethylsiloxane composites with carbon fiber. *Composites Communications*, **17**, 141–146 (2020).
<https://doi.org/10.1016/j.coco.2019.12.004>
- [25] Zhang C., Zhang C., Huang R., Gu X.: Effects of hollow microspheres on the thermal insulation of polysiloxane foam. *Journal of Applied Polymer Science*, **134**, 44778 (2017).
<https://doi.org/10.1002/app.44778>
- [26] Woldesenbet E.: Low velocity impact properties of nanoparticulate syntactic foams. *Materials Science and Engineering: A*, **496**, 217–222 (2008).
<https://doi.org/10.1016/j.msea.2008.05.024>
- [27] Shi Z., Zhao G., Zhang L., Wang G.: Lightweight, strong, flame-retardant PVDF/PMMA microcellular foams for thermal insulation fabricated by supercritical CO₂ foaming. *Composites Part B: Engineering*, **230**, 109554 (2022).
<https://doi.org/10.1016/j.compositesb.2021.109554>
- [28] Ge T., Zhang M., Tang K., Tang H.: Diisocyanate-modified graphene oxide/hydroxyl-terminated silicone rubber composites for improved thermal conductivity. *Materials Chemistry and Physics*, **252**, 123250 (2020).
<https://doi.org/10.1016/j.matchemphys.2020.123250>
- [29] Cheng W-C., Hsieh Y-T., Liu W-R.: Enhanced thermal conductivity of silicone composites filled with few-layered hexagonal boron nitride. *Polymers*, **12**, 2072 (2020).
<https://doi.org/10.3390/polym12092072>
- [30] Kuo C-F. J., Dewangga G. R. S., Chen J-B.: Fabrication of a thermally conductive silicone composite by incorporating surface-modified boron nitride. *Textile Research Journal*, **89**, 2637–2647 (2018).
<https://doi.org/10.1177/0040517518798654>
- [31] Wei Q., Yang D.: Formation of thermally conductive network accompanied by reduction of interface resistance for thermal conductivity enhancement of silicone rubber. *ACS Applied Electronic Materials*, **4**, 3503–3511 (2022).
<https://doi.org/10.1021/acsaelm.2c00475>
- [32] Li J., Li F., Zhao X., Zhang W., Li S., Lu Y., Zhang L.: Jelly-inspired construction of the three-dimensional interconnected BN network for lightweight, thermally conductive, and electrically insulating rubber composites. *ACS Applied Electronic Materials*, **2**, 1661–1669 (2020).
<https://doi.org/10.1021/acsaelm.0c00227>
- [33] Ouyang Y., Li X., Tian H., Bai L., Yuan F.: A novel branched Al₂O₃/silicon rubber composite with improved thermal conductivity and excellent electrical insulation performance. *Nanomaterials*, **11**, 2654 (2021).
<https://doi.org/10.3390/nano11102654>
- [34] Zhao L., Shi X., Yin Y., Jiang B., Huang Y.: A self-healing silicone/BN composite with efficient healing property and improved thermal conductivities. *Composites Science and Technology*, **186**, 107919 (2020).
<https://doi.org/10.1016/j.compscitech.2019.107919>
- [35] Wang J., Ni L., Li Q., Wu C.: The synergistic effects of carbon black and carbon fibre on the thermal conductivity of silicone rubber. *Polymers and Polymer Composites*, **23**, 271–275 (2014).
<https://doi.org/10.1177/096739111502300408>
- [36] Chiu H-T., Liu Y-L., Lin C-W., Shong Z-J., Tsai P-A.: Thermal conductivity and electrical conductivity of silicone rubber filled with aluminum nitride and aluminum powder. *Journal of Polymer Engineering*, **33**, 545–549 (2013).
<https://doi.org/10.1515/polyeng-2013-0025>
- [37] Song J., Wu L., Zhang Y.: Thermal conductivity enhancement of alumina/silicone rubber composites through constructing a thermally conductive 3D framework. *Polymer Bulletin*, **77**, 2139–2153 (2020).
<https://doi.org/10.1007/s00289-019-02839-3>
- [38] Liu C., Wu W., Drummer D., Shen W., Wang Y., Schneider K., Tomiak F.: ZnO nanowire-decorated Al₂O₃ hybrids for improving the thermal conductivity of polymer composites. *Journal of Materials Chemistry C*, **8**, 5380–5388 (2020).
<https://doi.org/10.1039/c9tc06805h>
- [39] Huang C., Wang Y., Cheng Y., Qi Z., Liu A., Deng Q., Hu N.: Naturally dried superelastic bioinspired graphene aerogel for pressure/stretch sensing and separation. *Composites Science and Technology*, **226**, 109549 (2022).
<https://doi.org/10.1016/j.compscitech.2022.109549>